JOURNAL OF AIRCRAFT
Vol. 38, No. 3, May–June 2001

Numerical Simulation of Enhanced Mixing in Jet Plumes Using Pulsed Blowing

Timothy D. Smith* and Alan B. Cain†
The Boeing Company, St. Louis, Missouri 63166
and
Clarence F. Chenault‡
Air Force Research Laboratory, Wright–Patterson Air Force Base, Ohio 45433

Pulsed jet blowing for mixing enhancement in a hot jet is examined using numerical simulation. Numerical simulations have been completed for a subscale turbojet engine, a full-scale ground demonstration case, and a high-bypass-ratio engine. These simulations have shown that pulsed jet blowing can significantly reduce jet plume potential core lengths at static and forward flight conditions. The numerical scheme uses large time-step implicit integration for efficiency and a second-order physical space algorithm for robustness. The pulsed jet disturbance is calculated directly, and a turbulence model is employed to represent the cascade to smaller length scales. Experimental data corresponding to the numerical simulations are also presented and indicate similar benefits from pulsed jet mixing.

Introduction

ACTIVE flow control technology is currently being evaluated for application in many areas of aircraft development. Performance of high-lift systems for transport and combat aircraft could be enhanced by modifying the effective aerodynamic shape of an airfoil or flap. Aircraft designed for minimum radar cross section may benefit from thrust vectoring by fluidic injection because control-surface deflections could be minimized or eliminated. Boundary-layer separation in advanced compact inlets and diffusers can be minimized with the application of synthetic or pulsed jets at the appropriate locations. Control of cavity acoustics with pulsed jets has also been demonstrated by Shaw.[1]

An application that has shown particular promise for active flow control technology is the enhanced mixing of a jet plume. For the case of large transport aircraft, three benefits can be realized from the active control of the jet plumes. One is the elimination of the need for a core thrust reverser for engine running off-load and backing operations because the core reverser is used primarily for the thermal protection of personnel loading and/or off-loading cargo aft of the aircraft. Second is the reduction of flap temperatures while operating in the powered lift portion of the flight envelope. This benefit could lead to the flap surfaces being constructed of lower cost and lighter weight materials. Third is an improved flap capture area for better, powered lift field length performance.

The benefits (and limitations) of active control of jet plumes have recently been investigated experimentally in research efforts conducted by the Boeing Company and the U.S. Air Force. In one case the centerline plume temperature reduction was measured for a subscale, single-exhaust, turbojet engine, the J402-CA-700 (nozzle diameter of 6 in.), while under the influence of an opposing pair of pulsed jets near the external nozzle lip. In a second experiment a full-scale JT8D-15 mixed-exhaust turbofan engine was modified to bleed air from the compressor to an array of pulsed jets located internally near the nozzle exit. The experimental setup for the JT8D is shown in Fig. 1. Concurrent with the JT8D testing, an effort was undertaken to develop a computational methodology for the prediction of plume flowfields incorporating the unsteady pulsed-jet technology demonstrated experimentally. This methodology, once validated, could be used to complement the experimental results and further the understanding of this technology. After validation is demonstrated with the results from the J402 and the JT8D simulations, this methodology is applied to an high-bypass-ratio-engine (HBRE) configuration with separate exhausts flow paths utilizing takeoff mass-flow rates.

To simulate flowfields of this nature, large time-step implicit integration is utilized for efficiency. There is no attempt to directly resolve all temporal and spatial scales. The grid resolution and time-step for the calculation is sufficient to resolve the large-scale forced disturbance of the pulsed jet. A turbulence model is employed to represent the cascade to smaller scales. Because the turbulence model includes large-scale turbulence effects, one should expect this approach to overpredict mixing. For each of the nozzle flows, a steady-state (unforced) calculation is completed, and then a forced calculation is initiated beginning from the steady-state solution.

Governing Equations

The Boeing (formerly McDonnell Douglas) compressible flow solver NASTD (Navier–Stokes time dependent), developed by Bush,[2] is used. The second-order physical space formulation of the spatial algorithm used for the present study is described in Cain and Bush.[3] NASTD is the precursor to the WIND flow solver available through the National Project for Applications-Oriented Research in Computational Fluid Dynamics (NPARC) Alliance. The NASTD flow solver incorporates an unsteady arbitrary inflow boundary condition to simulate the pulsed-jet flow. In this case the boundary condition is applied at the location of the pulsed-jet nozzle exit, and thus the flow within the pulsed jet system is not modeled. One, or more, of several fluid properties can be allowed to vary to simulate the pulsed jet. The unsteady fluid property varies in a sinusoidal fashion according to

$$P(t) = Po + \Delta P \cos(\omega t + \varphi)$$

where Po denotes the average of the fluid property, ΔP the amplitude of the perturbation, ω the angular frequency, and φ the phase angle.

Grid Generation

The grid-generation software MACGS, developed by Gatzke et al.,[4] is used to construct the three-dimensional computational

Received 3 June 1999; revision received 29 August 2000; accepted for publication 8 September 2000.

*Senior Project Engineer, Phantom Works. Member AIAA.
†President, Innovative Technology Applications Company, Chesterfield, Missouri. Associate Fellow AIAA.
‡ACE Control Program Manager, Air Vehicles Directorate; Clarence.chenault@va.afrl.af.mil. Senior Member AIAA.

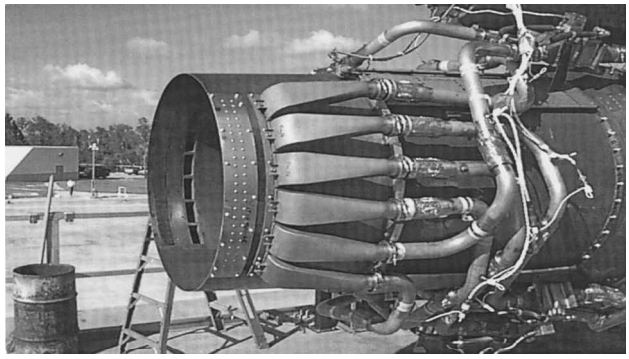

Fig. 1 JT8D full-scale engine pulsed jet experimental setup.

grids for the J402, JT8D, and HBRE simulations. To simplify the grid-generation process, the geometries of the J402, JT8D, and HBRE were assumed to be axisymmetric. For example, a nozzle plug support structure was not included in any of the cases. Thus, all of the computational zones are constructed by a simple rotation about the nozzle axis.

For the nozzle cases under consideration, the domain of interest is assumed to be 5 to 10 nozzle diameters downstream of the nozzle exit. As such, the downstream outflow boundary is placed at least 20 jet diameters downstream of the nozzle exit to prevent any influence of the downstream boundary in the domain of interest. Minimal grid stretching, e.g., 6 to 8%, in the axial direction is employed to properly resolve the primary forced disturbance. The maximum grid spacing is limited to 1/15 of the characteristic wavelength λ in the first 10 jet diameters downstream of the jet exit. The characteristic wavelength of the disturbance for the static round jet is given by

$$\lambda = 0.6\, u\text{jet}/f$$

where $u$jet is the fluid velocity at the nozzle exit and f is the pulse frequency in hertz. The Strouhal number, a dimensionless scaling parameter for this type of calculation, is defined as

$$St = \frac{f^* D\text{jet}}{u\text{jet}}$$

where Djet is the diameter of the nozzle exit.

Time Step

The solution timestep Δt is tied to the frequency f of the pulsed jets and the stability requirement of the flow solver. It is the stability requirement that sets the maximum allowable time step for the particular spatial and temporal scheme. The time step also must resolve the unsteady flow of the pulsed jet, however, with at least 100 time steps per pulse. Thus,

$$\Delta t = \frac{\Delta y \min(CFL)}{(u\text{jet} + a\text{jet})} = \frac{1}{(\#\text{timesteps/pulse})^* f}$$

The time step is adjustable, to a certain extent, through the minimum grid spacing Δy min. The minimum grid spacing, however, is constrained to resolve the smallest features of the nozzle geometry, pulsed-jet nozzle exit, and the forced disturbance in the plume.

Turbulence Model

For these calculations the Menter[5] blended k–ε/k–ω shear-stress transport (SST) turbulence model is used. For free shear layers this model is virtually identical to the Jones–Launder[6] k–ε model for free shear layers.

Results

An example of the computational grid for the J402 turbojet engine nozzle is shown in Fig. 2a. The nozzle exit is at $x = 6.86$ in. The nozzle walls are embedded in the grid clustering in the lower and upper left of the figure. This clustering becomes the clustering for the

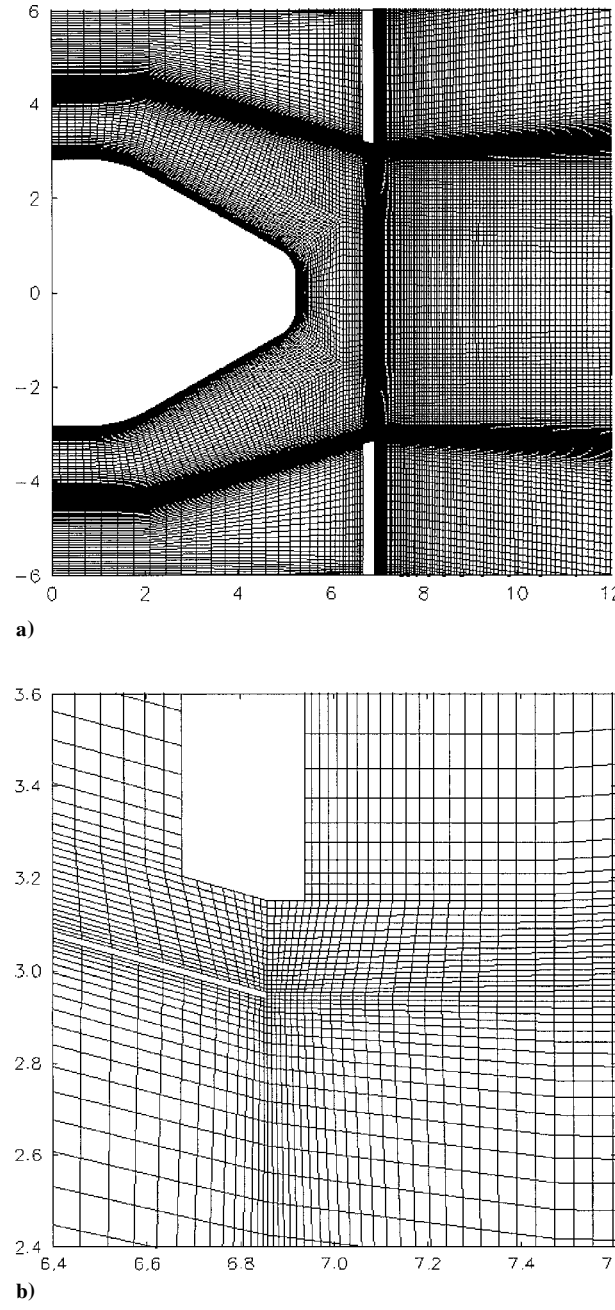

Fig. 2 J402 computational grid in the region of the a) nozzle exit, and b) nozzle lip and externally pulsed jet.

nozzle shear layers downstream of the nozzle exit. The nozzle plug and the external annular ring that contains the pulsed jets occupy the space not filled with grid. Topologically, the grid is five zones and 1.144 million grid nodes. The minimum spacing of the grid is 0.0075 in. Figure 2b shows more grid detail near the nozzle exit and pulsed jet. The minimum grid spacing is in this region near the nozzle exit. The pulsed jet is modeled with an arbitrary inflow boundary condition across four grid points at $y = 3.15$ in. The pulsed-jet width is 0.063 in. located just external to the nozzle exit. Both the upper and lower pulsed jet occupy 90 deg of circumferential arc.

The computational grid for the full-scale JT8D-15 mixed-flow turbofan engine nozzle is shown in Fig. 3a. The nozzle exit is at $x = 0.0$ in. The split between the core and fan flow is evident at about $y = \pm 15.0$ in. on the far left where the two streams enter the domain. The pulsed jets are located on the internal wall of the nozzle approximately 2 in. upstream of the nozzle exit. Topologically, the grid is eight zones and 1.48 million grid nodes. The minimum spacing for this grid is 0.025 in. A close-in view of the grid near the

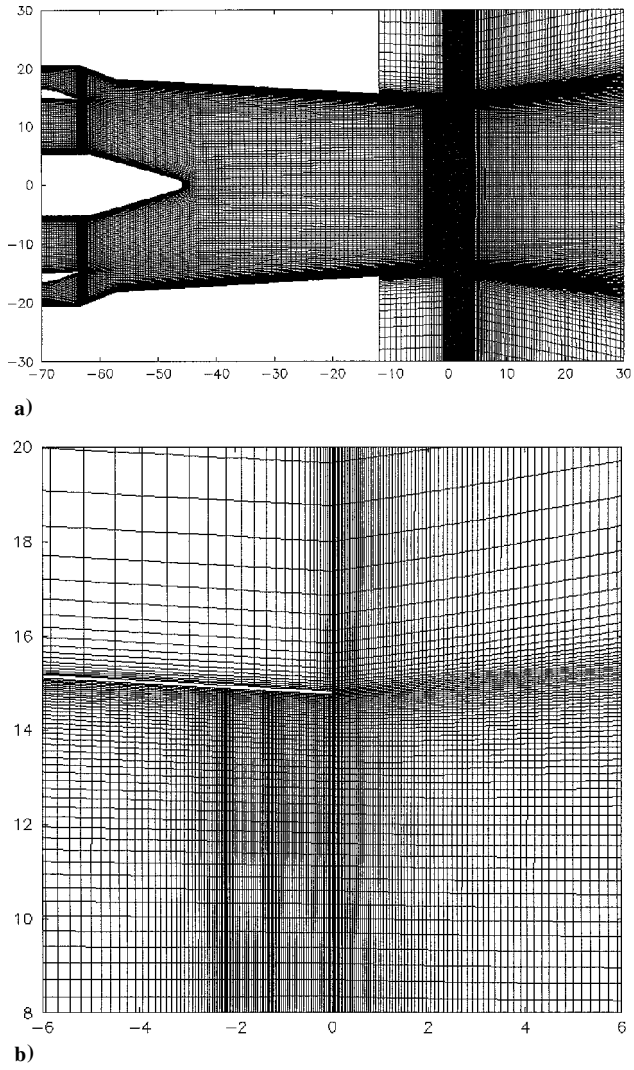

Fig. 3 JT8D computational grid in the region of the a) nozzle exit, and b) nozzle lip and externally pulsed jet.

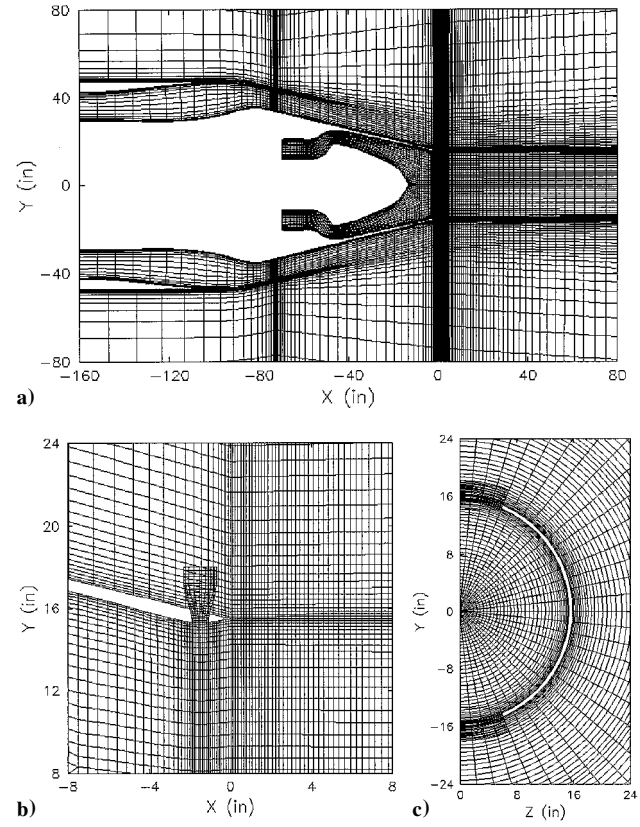

Fig. 4 HBRE computational grid in the region of the a) nozzle exit, b) nozzle lip, and c) external pulsed jet.

pulsed jet and nozzle exit is shown in Fig. 3b. Each of the pulsed jets (upper and lower) has a width of 0.925 in. and occupies 90 deg of circumferential arc.

The computational grid for the full-scale HBRE separate-exhaust flow turbofan engine nozzle is shown in Fig. 4a. The primary (core) nozzle exit is at $x = 0.0$ in., with a radius of about 15 in. The secondary (fan) nozzle exit is upstream of the primary nozzle exit at about $x = -80.0$ in., with an outer radius of approximately 40 in. Topologically, the grid is 13 zones and just over one million grid nodes. The minimum spacing for this grid is 0.10 in. Unlike the modeling done for the J402 and JT8D, a simplified model of the pulsed-jet injector is included for the case of the HBRE. This is done to better simulate the flowfield in the region of the pulsed-jet exit and the primary nozzle by removing the pulsed-jet boundary condition from the nozzle wall. A close-in view of the grid near the pulsed jet and nozzle exit is shown is Fig. 4b. The pulsed jet exit is 1.5 in. upstream of the primary nozzle exit. Each of the pulsed jets (upper and lower) has a width of 0.80 in. and occupies 45 deg of circumferential arc. An axial cut through the grid at $x = -1.5$ is shown in Fig. 4c. The physical domain of the pulsed-jet injector zones (upper and lower) indeed overlaps the primary nozzle external zone. This overlap, however, is visual only. Computationally, these zones are disconnected.

Pulsed-Jet Model

There is more than one way to specify the pulsed-jet flow for these calculations. NASTD/WIND allows for time varying Mach number, pressure (total or static), temperature (total or static), angle of attack, angle of yaw, or velocity, at an arbitrary inflow boundary. The user may even specify a combination of any, or all, of these flow variables. From the experimental results details of the pulsed-jet flow, e.g., Mach-number variation at the pulsed-jet exit, were not available. (Previous experimental work that provides a meaningful reference for the present study includes the investigations of Kibens,[7] Wlezien and Kibens,[8] and Parekh et al.[9]) The total mass flow of the pulsed-jet system, however, was known. Assuming a constant static pressure at the pulsed-jet exit, an average Mach number (and temperature) of the pulsed jet is deduced. The variation in Mach number, however, is subjective. For both the J402 and the JT8D configuration the pulsed jets consisted of an opposing pair covering 90 deg of circumferential arc for each jet, pulsed harmonically, 180 deg out of phase.

For the case of the J402, the fluctuation of the pulsed-jet exit Mach number from the average Mach number was $\pm 38\%$ (Mach $= 0.66 \pm 0.25$). A plot of the pulsed-jet mass flow over one cycle is shown in Fig. 5a. The total mass flow for the pulsed-jet system is 0.21 lbm/s, or approximately 3% of the primary nozzle flow.

For the JT8D the fluctuation of the pulsed-jet exit Mach number from the average Mach number was $\pm 72\%$ (Mach $= 0.58 \pm 0.42$). For this case a plot of the pulsed-jet mass flow over one cycle is shown in Fig. 5b. The total mass flow for the pulsed-jet system is 6.53 lbm/s, again approximately 3% of the primary nozzle flow.

For the HBRE the boundary condition for the pulsed jet is applied differently than the preceding cases because the actual pulsed jet is being modeled. A harmonically varying total pressure is applied at the inflow of the pulsed-jet model. Thus, the Mach-number variation at the pulsed jet exit is dependent on the supply total pressure. For this case the variation was on the order of 0.1 at minimum mass flow and 0.5 at maximum mass flow. A plot of the pulsed-jet mass flow over one cycle is shown in Fig. 5c. The total mass flow for the pulsed-jet system is 2.84 lbm/s, or approximately 1.5% of the primary nozzle flow.

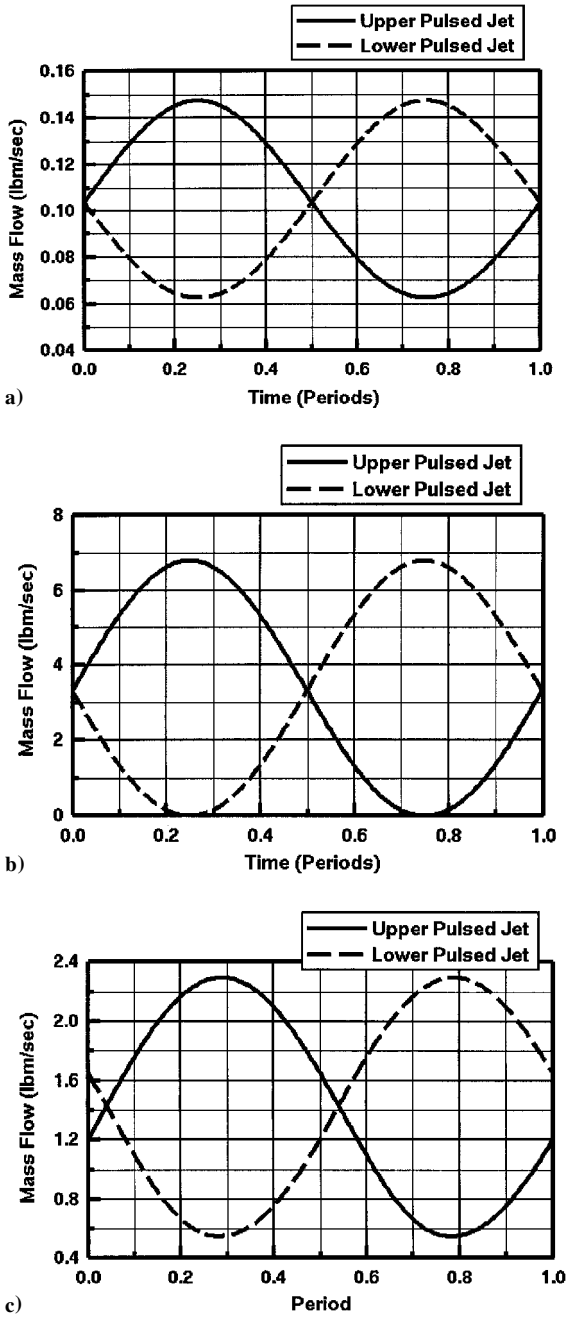

Fig. 5 Mass flow for the pulsed-jet systems over one cycle a) J402, b) JT8D, and c) HBRE.

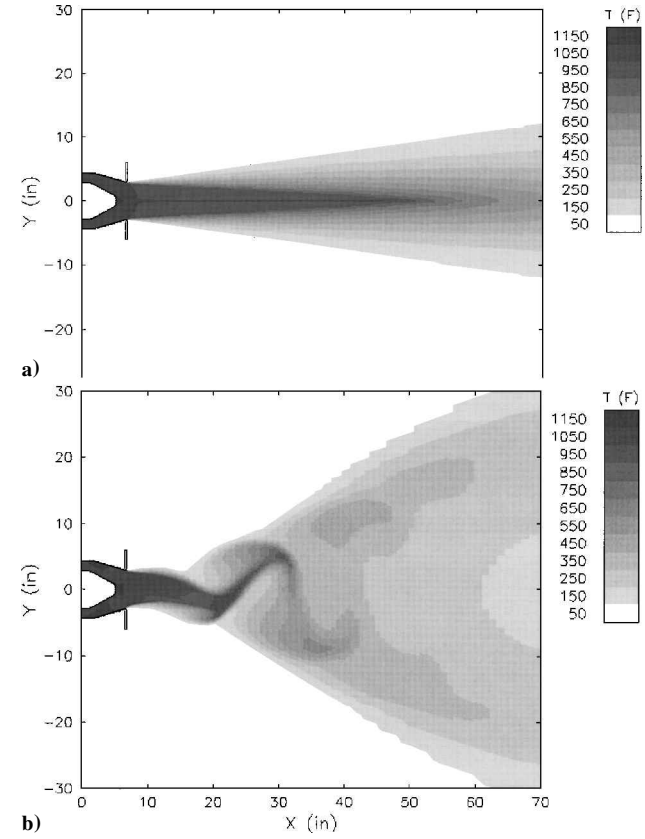

Fig. 6 Static temperature (°F) contours from the J402 simulation a) unforced (steady-state), and b) snapshot of the flapping plane at maximum mass flow of the lower pulsed jet.

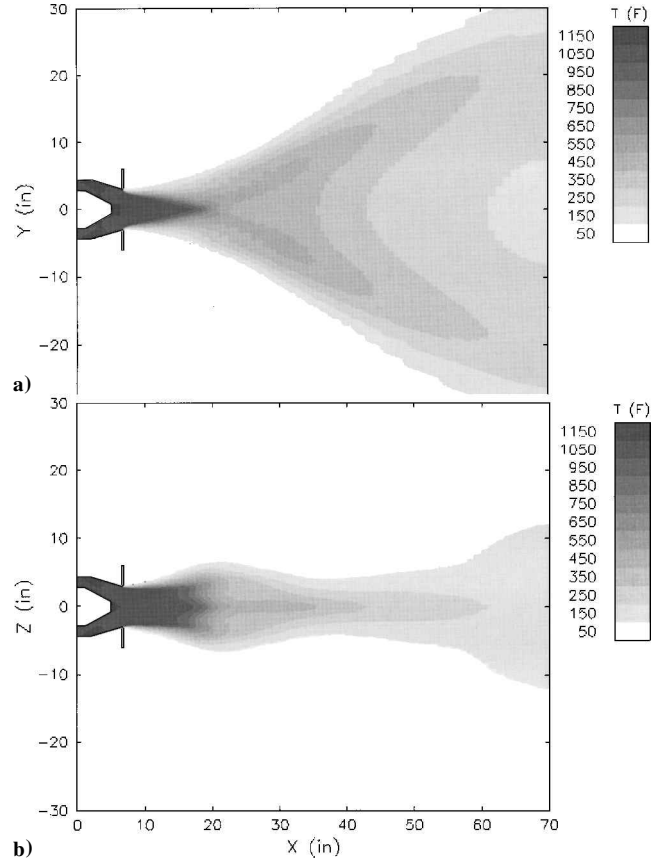

Fig. 7 Time-averaged static temperature contours from the J402 forced simulation a) flapping plane, and b) transverse plane.

J402 Simulation Results (Single Exhaust)

Qualitative comparisons of the effects of pulsed-jet mixing for the J402 are shown in Fig. 6. The contours are of static temperature. Figure 6a shows an unforced or steady-state simulation of the plume. A snapshot in time of the forced simulation is shown in Fig. 6b. In this view the cut is through the plume centerline and the circumferential midpoint of the pulsed jets and depicts the flapping mode of the simulation. In this configuration the amplitude of the flapping plume is well in excess of the nozzle exit diameter. Time-averaged static-temperature contours are shown in Fig. 7. Figure 7a shows the flapping plane, which is essentially the time average of the flapping depicted in Fig. 6b. Figure 7b is a view of the transverse plane, or the plane perpendicular to the flapping plane, and does not cut through either of the opposing pulsed jets.

Quantitative comparisons of the time-averaged static and total temperature along the plume centerline for the computational and experimental results are shown in Fig. 8. Beginning at two nozzle

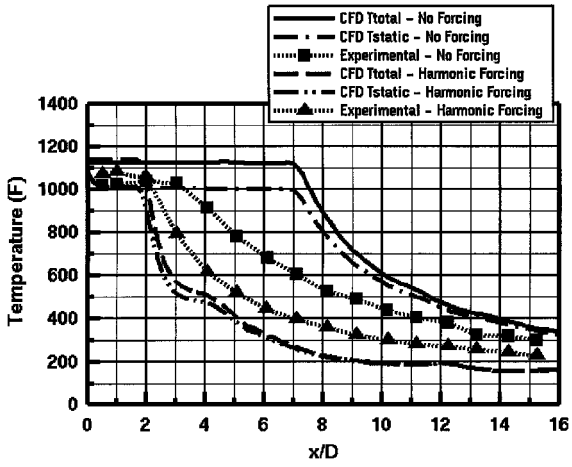

Fig. 8 Time-averaged plume centerline temperatures for the J402.

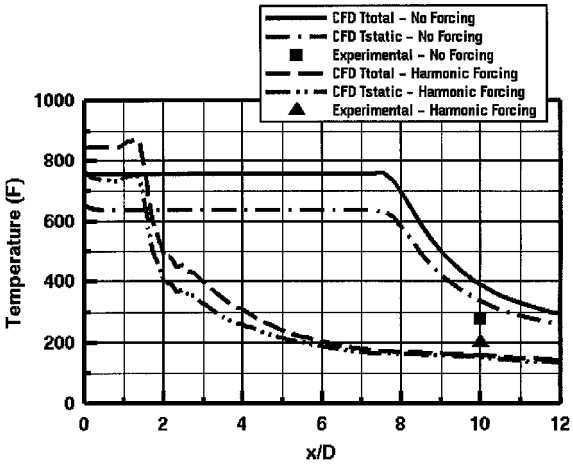

Fig. 9 Time-averaged plume centerline temperatures for the JT8D.

diameters downstream, the computational results predict a dramatic temperature reduction along the plume centerline. At five nozzle diameters downstream a temperature reduction of 600 deg is predicted. The experimental results show a similar trend. Discrepancies between the computational and experimental results are expected as a result of the simplification of the geometry and flow conditions of the computational model, particularly those of the pulsed jet.

JT8D Simulation Results (Mixed Exhaust)

Quantitative comparisons of the time-averaged static and total temperature along the JT8D plume centerline for the computational and experimental results of are shown in Fig. 9. As in the case of the J402, beginning at roughly two nozzle diameters downstream the computational results predict a dramatic temperature reduction along the plume centerline. At six nozzle diameters downstream a reduction in total temperature of 550 deg is predicted. The experimental results for this case are shown at 10 nozzle diameters downstream of the nozzle exit.

Notice for this case a marked increase in the static and total temperature of the primary nozzle flow at the nozzle exit. The increase in the total temperature is caused by bleeding the primary engine flow as a source for the pulsed-jet flow. The bleeding of the engine also results in a 4% reduction in total pressure of the core flow. The combination of these two effects increases the static temperature on the plume centerline at the nozzle exit roughly 100°F. This effect can be seen in the first two nozzle diameters downstream of the nozzle exit.

Similar qualitative comparisons for the JT8D are shown in Fig. 10. As before, contours of static temperature are shown. Figure 10a shows the unforced or steady-state simulation. Figure 10b depicts

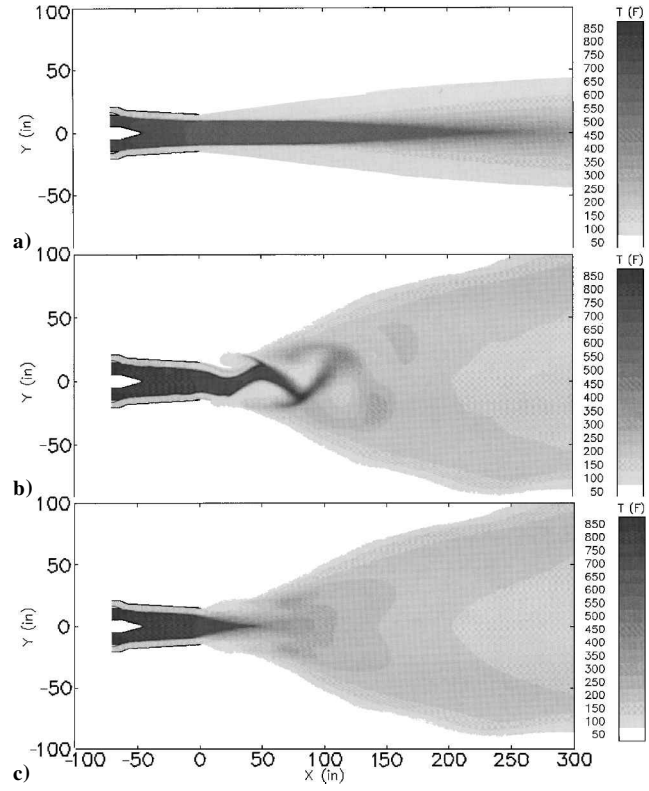

Fig. 10 Static temperature (F) contours from the JT8D simulations a) unforced (steady state), b) snapshot of the forced simulation in the flapping plane at maximum mass flow of the upper pulsed jet, and c) time average of the forced simulation in the flapping plane.

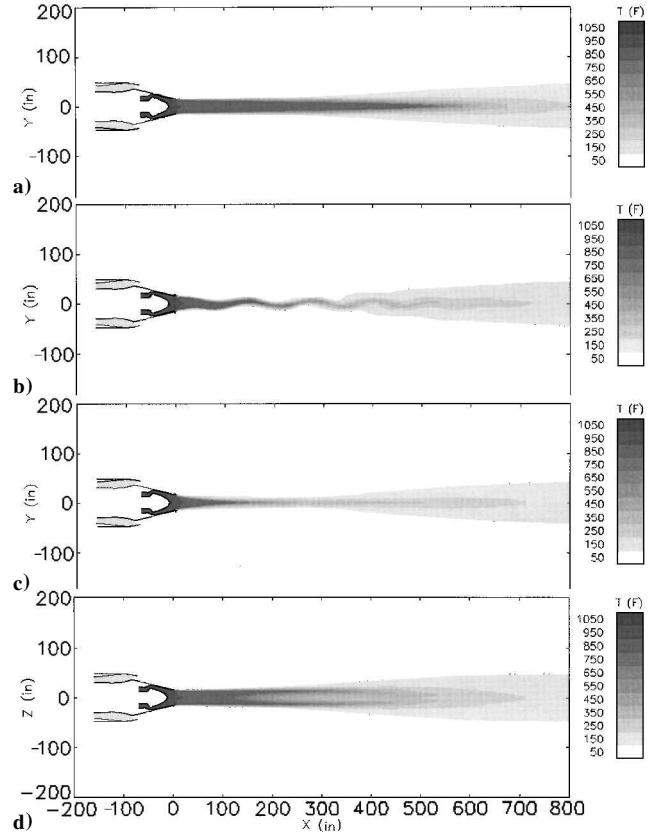

Fig. 11 Static temperature (F) contours from the HBRE simulations a) unforced (steady state), b) snapshot of the forced simulation in the flapping plane, c) time average of the forced simulation in the flapping plane, and d) time average of the forced simulation in the transverse plane.

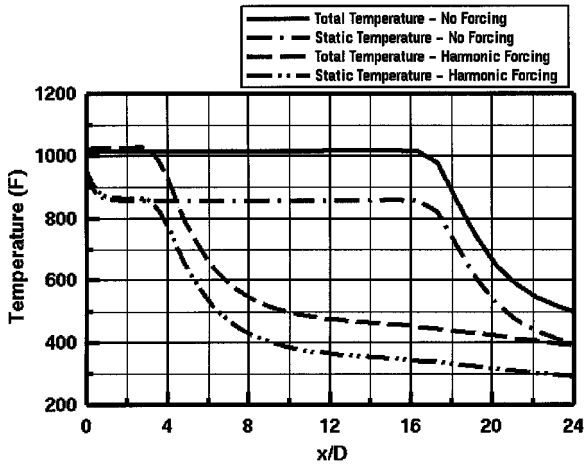

Fig. 12 Time-averaged plume centerline temperatures for the HBRE.

a snapshot of the forced simulation in the flapping plane, the plane that contains a cut through the pulsed jets. As was the case in the J402 simulation, the amplitude of the flapping plume exceeds the nozzle exit diameter. Figure 10c is the time-averaged static contour levels for the plume in the flapping plane.

HBRE Simulation Results (Separate Exhausts)

The HBRE simulation is the only one of the calculations done for a forward flight condition, specifically, a takeoff condition at sea level with a freestream Mach number of 0.24. The primary flow NPR is 1.52 with a total temperature of 1014°F. The secondary flow NPR is 1.72 with a total temperature of 157°F.

Once again, qualitative comparisons similar to the J402 and JT8D simulations are shown in Fig. 11. As before, contours of static temperature are shown. Figure 11a shows the unforced or steady-state simulation predictions. Figure 11b depicts a snapshot of the forced simulation in the flapping plane, the plane that contains a cut through the pulsed jets, and Figs. 11c and 11d are the time-averaged static contour levels for the plume in the flapping plane and transverse plane, respectively.

Quantitative comparisons of the time-averaged static and total temperature along the HBRE configuration's centerline are shown in Fig. 12. The diffusion of the core exhaust plume of the HBRE configuration is significantly slower than that observed for the cases of the J402 and JT8D. This is because of the influence of the secondary flow that envelops the core flow. One effect of the secondary flow is to increase the convection velocity of the disturbance responsible for mixing, thus increasing the distance downstream of the core nozzle exit where significant temperature reduction along the plume centerline is evident.

An additional effect of the secondary flow is depicted in Fig. 11d. The mixing of the plume is naturally most effective in the geometric plane that contains the pulsed jets, the flapping plane. In the plane perpendicular to the flapping plane, the transverse plane, the plume has a natural tendency to bifurcate. For the J402 and JT8D, with no secondary flow, the bifurcation is minimal. For the HBRE the secondary flow exasperates the bifurcation. Future work will focus on optimizing the pulsed-jet configuration, particularly for the HBRE.

Conclusions

An efficient computational methodology has been developed for the analysis of unsteady pulsed-jet mixing flowfields. The benefits of pulsed-jet mixing at sea-level static conditions are evident in the reduction of plume centerline temperatures aft of approximately two to three nozzle diameters downstream of the nozzle exit. Furthermore, significant differences in plume expansion characteristics are observed between single-and mixed-exhaust configurations and separate-exhaust configurations.

Acknowledgments

The authors would like to thank Steven H. Walker for initiating this work and Yvette Weber of the Air Force Research Laboratory for their support as government program managers and comments on this effort. In addition, the efforts and support of John Dorris III, David Smith, and Doug Wiese, all of the Boeing Company, were essential to the success of this work. Funding for this investigation was provided by the Air Force Research Laboratory and the Joint Technical Coordination Group for Aircraft Survivability.

References

[1]Shaw, L., "Active Control of Cavity Acoustics," AIAA 98-2347, June 1998.

[2]Bush, R. H., "A Three Dimensional Zonal Navier–Stokes Code for Subsonic Through Hypersonic Propulsion Flowfields," AIAA Paper 88-2830, July 1988.

[3]Cain, A. B., and Bush, R. H., "Numerical Wave Propagation Analysis for Stretched Grids," AIAA Paper 94-0172, Jan. 1994.

[4]Gatzke, T. G., LaBozzetta, W. F., Finfrock, G. P., Johnson, J. A., and Romer, W. W., "MACGS: A Zonal Grid Generation System for Complex Aero-Propulsion Configurations," AIAA Paper 91-2156, June 1991.

[5]Menter, F. R., "Zonal Two Equation k-ε Turbulence Models for Aerodynamic Flows," AIAA 93-2906, July 1993.

[6]Jones, W. P., and Launder, B. E., "The Calculation of Low-Reynolds-Number Phenomena with a Two-Equation Model of Turbulence," *International Journal of Heat and Mass Transfer*, Vol. 16, 1973, pp. 1119–1130.

[7]Kibens, V., "Discrete Noise Spectrum Generated by an Acoustically Excited Jet," *AIAA Journal*, Vol. 18, No. 4, 1980, pp. 434–441.

[8]Wlezien, R. W., and Kibens, V., "Influence of Nozzle Asymmetry on Supersonic Jets," *AIAA Journal*, Vol. 26, No. 1, 1988, pp. 27–33.

[9]Parekh, D. E., Kibens, V., Glezer, A., Wiltse, J. M., and Smith, D. M., "Innovative Flow Control—Mixing Enhancement Experiments," AIAA Paper 96-0308, Jan. 1996.